# Predicting the yield of ion pair formation in molecular electrical doping: redox-potentials *versus* ionization energy / electron affinity

Berthold Wegner[1,2], Lutz Grubert[3], Dennis Chercka[4], Andreas Opitz[2], Adriana Röttger[2], Yadong Zhang[5], Stephen Barlow[5], Seth R. Marder[5], Stefan Hecht[3], Klaus Müllen[4], and Norbert Koch[1,2]*

[1] Helmholtz-Zentrum Berlin für Materialien und Energie GmbH, Albert-Einstein-Str. 15, 12489 Berlin, Germany
[2] Institut für Physik & IRIS Adlershof, Humboldt-Universität zu Berlin, Brook-Taylor-Str. 6, 12489 Berlin, Germany
[3] Institut für Chemie, Humboldt-Universität zu Berlin, Brook-Taylor-Straße 2, 12489 Berlin, Germany
[4] Max-Planck-Institut für Polymerforschung, Ackermannweg 10, 55128 Mainz, Germany
[5] School of Chemistry and Biochemistry and Center for Organic Photonics and Electronics (COPE), Georgia Institute of Technology GA, Atlanta 30332-0400, USA

**Abstract**

Efficient electrical doping of organic semiconductors relies on identifying appropriate molecular dopants that are capable of ionizing semiconductor molecules with a high yield, thereby creating mobile charges. We explore the suitability of two different material parameters to predict ion pair formation for different sets of semiconductor-dopant combinations: (i) redox-potentials measured by cyclic voltammetry in solution and (ii) ionization energy (IE) / electron affinity (EA) measured on thin films by ultraviolet / inverse photoelectron spectroscopy. Our study suggests, at least for molecular semiconductors and dopants, that redox-potentials are better suited to identify matching material pairs and their ion pair formation yield than IE/EA values. This is ascribed to the dependence of IE/EA values on molecular orientation and film structure on and above the meso-scale. In contrast, cyclic voltammetry measurements, although performed on solution rather than on thin films, capture dopant-semiconductor energy levels on the molecular scale, which is more relevant for doping even in the case of solid thin films.

**Introduction**

Doping is a key technological method to control the charge carrier density and Fermi level position in semiconductors. For organic semiconductors, the use of strong molecular electron donors (acceptors) as dopants for n-type (p-type) doping has emerged as suitable approach,[1–10] often termed “electrical doping”. In analogy to doping of classical inorganic semiconductors, the dopant molecules should become ionized, creating excess charges of opposite sign in the semiconductor host. This process requires an adequate energy alignment of the respective frontier molecular orbital levels to facilitate the formation of dopant-host ion pairs (IPAs). To select proper dopant/host pairs, part of the research community relies on comparing ionization energy (IE) and electron affinity (EA) values measured *via* ultraviolet and inverse photoelectron spectroscopy (UPS and IPES) on thin solid films.[2–4,6–9] For instance, in the case of p-type doping, the EA of the dopant should be higher than the IE of the host for IPA formation. Since IE/EA values determined by UPS/IPES represent the respective energies of charged species in a matrix of neutral molecules, this approach should predict the stability of charges in the host and ionized dopants at large distance from each other, with negligible Coulomb attraction between them – i.e. the energy required to form mobile charges. Alternatively, redox-potentials measured *via* cyclic voltammetry (CV) are also used for material selection.[10] One reservation for using CV data might be related to the notion that parameters determined in solution are not readily relevant for the solid, and the fact that solvent polarity and electrostatic effects of electrolytes can influence the measurement. Indeed, there are notable differences in the material properties that are captured by UPS/IPES and CV experiments, and the reliability of either data set for selecting dopant/host pairs is still an unresolved issue,

as both approaches have limitations.[11–15] One issue of using solid state IE/EA was recently demonstrated by computational work, where it was shown that the EA of a dopant molecule in a host semiconductor environment can differ by up to 1 eV from the EA of the pure dopant crystal as a result of intermolecular electrostatic interactions.[16] From their results, the authors concluded that comparing IE/EA of the pure phases of host and dopant is insufficient to predict IPA formation yield of the host/dopant system, as they find a tendency of systematically underestimating the $IE_{host} - EA_{dopant}$ difference (for p-doping) in this way. However, such computational approaches are quite involved and time-consuming, especially when large variations of specific host environments have to be sampled. In contrast, the aim of the present study is to examine experimentally the practicality of redox-potentials measured *via* CV in solution in comparison to IE/EA values measured *via* UPS/IPES on thin films to predict the yield of IPA formation. At this point it has to be noted that this investigation focuses entirely on the *ionization efficiency*, which is the yield of ionized host molecules per number of dopant molecules. *Doping efficiency*, on the other hand, is generally used to describe the yield of generated mobile charge carriers per number of dopant molecules. It is generally observed that ionization usually proceeds with high efficiency (up to 100% if host/dopant pairs are chosen adequately), whereas the yield of mobile charge carriers is much lower (on the order of 10%) for the typically high dopant-concentrations used with organic semiconductors (several mol%), in part at least due to above-mentioned Coulomb interactions between dopant ions and host ions.[17–19]

For clarity, we briefly revisit both experimental techniques and compare the differences in the measured values. In principle, both techniques measure the difference in total energy of a molecule between the N-electron ground state and the (N±1)-electron ionized state; however, there are fundamental differences in the involved ionization processes. In UPS, the IE is measured at the surface of a molecular solid (thin film) by irradiating the sample with photons and analyzing the kinetic energy of the emitted photoelectrons.[20] In IPES, the EA is measured in the essentially time-reversed process of UPS, where the sample is irradiated with electrons and the emitted photons are analyzed.[21] The measured IE (EA) corresponds to that of a nearly fully relaxed positive (negative) polaron. When a molecule embedded in the solid becomes ionized, it induces electronic polarization in the surrounding material, which screens the charge and, therefore, stabilizes the system, which is associated with an energy on the order of 1.0-1.5 eV.[22–24] Furthermore, reorganization of the nuclei of the ionized molecule (ca. 100 meV) and lattice relaxation of neighboring molecules (ca. 10 meV) occur. Due to timescale considerations, it is generally acknowledged that UPS (IPES) captures the electronic polarization but not intra- and inter-molecular reorganization, and thus the IE (EA) is over- (under-) estimated by up to 100 meV.[24] However, since UPS/IPES measure IE and EA at the surface of the solid, the polarization may differ from inside the bulk, and particularly surface dipoles (originating from the mutual arrangement of intramolecular dipoles) contribute to the measured values.[25] More importantly, for molecular and polymeric solids that are not perfectly amorphous, IE and EA values depend strongly on the orientation of molecules with respect to the surface. Collective electrostatic effects of the charge density distribution, including charge-permanent quadrupole and higher-multipole interactions, substantially modify the energy landscape, from molecular to macroscopic length scales.[26–29] In turn, depending on sample structure, IE and EA values for one material can differ by over 500 meV. Including these solid state effects, the IE/EA of a molecular thin film can be written as

$$IE_{film} = IE_{gas} - P_{+} - W_{+} \quad \text{and} \quad EA_{film} = EA_{gas} + P_{-} + W_{-}. \tag{1}$$

Here, $IE_{gas}/EA_{gas}$ is the IE/EA of the isolated molecules in the gas phase, $P_{\pm}$ the polarization energy, which always has a positive value (in general $P_{+} \neq P_{-}$), and $W_{\pm}$ (with positive or negative sign) includes orientation-dependent electrostatic effects and; in case of crystalline materials, also eventual dispersion of electron bands derived from the highest occupied molecular orbital (HOMO) or lowest unoccupied molecular orbital (LUMO).[29]

In CV, the oxidation/reduction potential ($E_{ox}/E_{red}$) of an analyte solution (usually in non-aqueous solvents) is measured by cyclically sweeping a potential between a working electrode and a reference electrode immersed

in the solution, while measuring the current response.[30] Commonly, the potential of any redox-process is measured as half-wave potential $E_{1/2}$ (the average between the peak potentials of forward and return potential sweep), which is a good estimate of the formal potential for reversible one-electron processes. However, since the potential is determined with respect to a reference electrode, the potential is only a relative measure of the ionization potential / electron affinity in solution. Reported potentials are typically referenced to a standard measured under the same experimental conditions, often the ferrocene/ferrocenium couple ($Fc/Fc^+$), since it has a well-defined redox-process and is stable in most employed solvents.[31] To calculate absolute values of the potentials, the potential of ferrocene with respect to the vacuum level has to be taken into account, which has been variously estimated to lie between -4.8 eV and -5.3 eV, this value itself usually relying on estimation of the absolute value of the NHE ($H_2/H^+$) potential.[32,33] Thus, it is generally preferable to compare relative values referenced against $Fc/Fc^+$ than to report absolute values. Similarly to the polarization energy in a thin film, which takes into account the environment of the charged molecule and its response, effects of solvent and electrolyte on the oxidation/reduction process of the molecule have to be considered. In analogy to equation (1), the IE/EA in solution can be related to the IE/EA in gas phase by

$$IE_{sol} = eE_{1/2}^{ox} + C = IE_{gas} - \Delta G_{solv}^{+} \quad \text{and} \quad EA_{sol} = eE_{1/2}^{red} + C = EA_{gas} + \Delta G_{solv}^{-}\,, \tag{2}$$

where $e$ is the elementary charge, C the absolute potential of the used standard or reference electrode in the given solvent, and $\Delta G_{solv}^{\pm}$ the total change in free energy of the oxidant and reductant upon solvation. Influences on the redox-potentials of different solvents and electrolytes are usually on the order of several 10 meV for typical molecular semiconductors and dopants, but can also reach values of a few 100 meV.[31,34] The method described above to determine the redox-potentials is valid for reversible reactions. When the redox-process is only quasi-reversible or even irreversible, the thermodynamically relevant formal potential cannot be reliably estimated. Determination of reliable values for polymers is also less straightforward;[33] solution voltammograms can be complicated by slow diffusion, while the apparent reversibility of that of films can be affected by relatively slow diffusion of charge-compensating electrolyte ions in and out of the films.

Although empirical linear relationships between the solid state IE (EA) and the oxidation (reduction) potential of molecular organic semiconductors[11–13,15] as well as polymers[35,36] have been reported, there is considerable scatter in plots of oxidation (reduction) potential *vs.* IE (EA). Thus, in individual cases, especially for non-amorphous materials, values can deviate by several 100 meV even up to 1 eV from the assumed relationship due to the above described particularities of the two methods. Additionally, the differences between $\Delta G_{solv}^{\pm}$ and $P_{\pm}$ are expected to strongly dependent on the size and shape of, as well as charge distribution in, the ions. Thus, the deviations seem too large to enable accurate prediction of IPA formation yield for individual host/dopant systems.

To investigate which data-set is more reliable for predicting the ion pair formation yield, we chose three different sets of host – dopant combinations, whose chemical structures along with their redox-potentials and solid state IE/EA are summarized in Figure 1. Set I (Figure 1a) consists of structurally similar molecules as donor host – acceptor dopant combinations (i.e., p-type doping) that differ in their $E_{ox}$/IE and $E_{red}$/EA, respectively. Structural similarity within this set was chosen to minimize the possible influence of molecular conformation variations. Accordingly, p-dopants were increasingly fluorinated tetracyanoquinodimethane derivatives ($F_x$TCNQ).[37,38] However, $F_x$TCNQs are known to also form ground-state charge transfer complexes (CPXs) with many organic semiconductors, where the frontier molecular orbitals overlap and give rise to a new set of hybrid orbitals of the complex.[19,39] For crystalline charge transfer salts, it has been recognized that slight changes in structure modify the local electrostatic potentials inside the solid, and due to the pronounced electron correlation in molecule-based materials this influences whether integer charge is transferred or only a fraction.[40] More recently, in the context of molecularly doped conjugated polymers, featuring much more structural variability than crystalline charge transfer salts, evidence for both charge transfer interactions, i.e.,

IPA and CPX formation was reported.[41–43] For the same system, either of the two was found, delicately depending on the relative position of conjugated segment and dopant. Because CPX formation results in particularly low doping efficiency[19], i.e., low yield of mobile charge carriers generated per dopant molecule, thus not favorable for applications, here we aim selectively at IPA cases (i.e., integer charge transfer between dopant and host). We chose two organic semiconductors with a twisted three-dimensional structure: *N,N*-di-p-methoxyphenylamine-substituted pyrene derivatives ($D_a$ and $D_b$); these have previously been used as hole-transport materials and are potentially electron donors with respect to the $F_x$TCNQs.[44,45] We assume that the arylamine groups lead to steric hindrance, prohibiting an overlap of the frontier orbitals with those of the dopants and thus avoiding the formation of CPXs. This approach is justified as we only found evidence for IPA formation in our experiments (*vide infra*).

Set II (Figure 1b) consists of α-sexithiophene (6T) and its more soluble, hexyl side-chain substituted derivative (DH6T) as donor hosts and molybdenum tris[1,2-bis(trifluoromethyl)ethane-1,2-dithiolene] [$Mo(tfd)_3$] as acceptor dopant. 6T and DH6T, previously used as semiconductor in organic field effect transistors (OFETs),[46–48] are known to adopt either a lying or standing orientation in thin films (monolayers or thin multilayers)[27,49] depending on the substrate onto which they are deposited, leading to a difference in IE of 600 meV.[50] $Mo(tfd)_3$ is used as a very potent p-dopant[51,52] and its bulky 3D-structure is likely to reduce the possibility of CPX formation.

Set III (Figure 1c) consists of perfluoropentacene (PFP) as acceptor host and cobaltocene ($CoCp_2$) as donor dopant (i.e., n-type doping). PFP, used as n-type semiconductor in OFETs,[53,54] is known to adopt orientations in thin films similar to 6T and DH6T, and standing *vs*. lying orientation result in a difference in the measured IE/EA of 540/650 meV, respectively.[28,29] $CoCp_2$ is typically used as a reducing agent in organometallic chemistry[31] and has also been shown to act as n-type dopant with a quite low IE of 4.1 eV.[55]

**Experimental**

The donors 1,3,6,8-tetra[bis(*p*-anisyl)amino]-4,5,9,10-tetramethoxypyrene ($D_a$), 1,3,6,8-tetra[bis(*p*-anisyl)amino]pyrene ($D_b$) and the p-dopant $Mo(tfd)_3$ were synthesized as described elsewhere.[56,57] The $F_x$TCNQ molecules were purchased from TCI Europe N.V., 6T and $CoCp_2$ from Sigma Aldrich GmbH, DH6T from H.C. Starck GmbH, and PFP from Kanto Denka Kogyo Co. Ltd. All materials were used without further purification. Stock solutions with concentrations of around $1\times10^{-3}$ M were prepared under nitrogen atmosphere in a glovebox (<0.1 ppm $H_2O$, <0.1 ppm $O_2$) using dry and degassed solvents (commercially available anhydrous solvents were further degassed via three freeze-pump-thaw cycles), unless otherwise stated. For set I and set III, solutions were prepared using dichloromethane (DCM), while chlorobenzene (CB) was used for set II. For the optical measurements of set I and set II, 100 µl of the donor stock solution were mixed with an appropriate amount of the respective acceptor stock solution (molar ratio of 1:1) and then filled with the respective solvent to a total volume of 300 µl. In this way, all of the measured mixtures contained the same concentration of donor / acceptor molecules; therefore, the optical spectra can be compared without normalization. For set III, saturated PFP solutions (< 0.1 mM) with non-dissolved PFP still being present were used and mixed with (excess) solutions of $CoCp_2$ (see SI for further discussion). Thin films for set I were prepared via drop-casting on solvent-cleaned and UV-ozone treated quartz glass substrates from (mixed) solutions. While we cannot formally prove that molecular-scale mixing in thin films proceeds, we have good indications from scanning force microscopy (SFM) that films based on $D_a$ and $D_b$ mixed with the $F_x$TCNQs do mix intimately even at 1:1 molar ratio, as no morphological differences between pure semiconductor films and mixed films can be observed (see example image in SI). For set II, thin films were prepared on quartz substrates via (co-) evaporation of the materials (in a molar ratio of 1:1) in a vacuum system with a base pressure of $3\times10^{-8}$ mbar using evaporation rates of around 0.3 Å $s^{-1}$. From SFM we find that pure $Mo(tfd)_3$ grows in large islands, while

pure 6T grows in more homogeneous films with grains of diameter in the range of 150 nm. The mixed film shows a morphology with protruding high features, and smaller grains in between (see SI). This indicates that 6T and $Mo(tfd)_3$ do mix to some extent (inducing the much smaller grain size of low-lying features), but phase-separated islands of $Mo(tfd)_3$ may coexist. Thin films of highly doped PFP (set III) were prepared by dipping vacuum-deposited thin films of PFP into a $CoCp_2$ solution or sequentially spin-coating[58] $CoCp_2$ on top of the PFP films (see SI for further discussion).

Optical absorption spectroscopy was performed using a Lambda 950 UV/Vis/NIR spectrophotometer (Perkin Elmer Inc.). The optical measurements on thin films were performed with the samples mounted in small nitrogen filled boxes with two quartz glass windows, sealed by using a vinyl gasket. A baseline spectrum of the boxes with a mounted clean quartz glass substrate was subtracted from the spectra before further analysis. For the optical measurements in solution quartz glass cuvettes with a path length of 1 mm were used, which were sealed under nitrogen atmosphere using a Teflon stopper. For some spectra (where stated), a background, taking into account Rayleigh scattering and arbitrary linear background, with the form $A = a + bE + cE^4$ was subtracted before analysis, where a, b, and c are arbitrary fitting parameters, A is the absorbance, and E is the photon energy.

Cyclic voltammetry was performed using a PG310 USB (HEKA Elektronik) potentiostat interfaced to a PC with PotMaster v2x43 (HEKA Elektronik) software for data evaluation. A three-electrode configuration was used containing a non-divided cell consisting of a platinum disc (d = 1 mm) as working electrode, a platinum plate as counter-electrode, and a saturated calomel electrode (SCE) with an agar-agar-plug in a Luggin capillary with a diaphragm as reference electrode. Measurements were carried out in 1 mM solutions in dichloromethane (HPLC-grade, dried over calcium hydride and distilled) containing 0.1 M $Bu_4NPF_6$ using a scan rate of $dE/dt = 1$ $Vs^{-1}$. Oxygen was removed by argon purging (Argon 99.999% ALPHAGAZTM 1 and ALPHAGAZ Purifier, Air Liquide). The potentials given are referenced to the half-wave potential of the ferrocene redox-couple ($Fc/Fc^+$), which has been used as external standard.

UPS measurements were performed at a base pressure of $5\times10^{-10}$ mbar using the HeI photon line (21.22 eV) of a gas discharge lamp. The spectra were collected in normal emission using a SPECS Phoibos 100 hemispherical electron energy analyzer with an energy resolution of 150 meV. For the determination of the work function, the secondary electron cut-off (SECO) was measured with the sample biased at −10 V to clear the analyzer work function. The onset of the HOMO and also the SECO were determined by the intersection of a horizontal baseline resembling a constant background and a line fitted to the linear part of the HOMO or SECO, respectively. Samples for UPS measurements were prepared via spin-coating (20 / 40 rps) of the respective DCM solutions onto solvent-cleaned and UV-ozone treated indium tin oxide (ITO) substrates under inert atmosphere.

**Results and Discussion**

In Figure 1 the redox-potentials (half-wave potentials measured by CV) and the solid-state IE/EA (onsets of energy levels measured by UPS/IPES) of the investigated materials are juxtaposed. Redox-potentials for set I were measured by CV (see Supplementary Information -SI) and IE for the donors $D_x$ were determined by UPS (see SI), while IPES values were taken from literature.[59] The energy levels for set II & set III were taken from literature.[29,31,51,53,55,60–62] (Note: IE values reported for 6T[61] and DH6T[62] were maxima of the HOMO-related peak, rather than onsets of ionization; the values used here are, however, the onset values and thus 400-500 meV lower than those in these two references). The values of the redox-potentials are consistent with previously reported values[63–66] (except PFP, where no literature data were available), whereas UPS/IPES data are only sparsely available. For 6T several other IE values have been reported, within the range of 4.6 eV to

5.3 eV, but the molecular orientation was not reported and we thus assumed polycrystalline samples.[67–70] In addition to the literature values for the EA of PFP thin films with strict standing and lying orientation, we also provide an "intermediate" EA value. Since the cause for the orientation-dependent EA of PFP is the surface electrostatic potential created by the collective effect of the highly polar C-F bonds in ordered molecular assemblies[28], the EA of a thin film with random molecular orientation is expected to be in between the values obtained for standing and lying orientation. In addition, one might suppose that the intermediate value (representative of an averaged electrostatic potential in the molecular proximity) might be more relevant for charge transfer with the dopant. Thus, the intermediate EA value was estimated to be around 3.8 eV, in analogy to the values reported for pentacene, where the EA in lying and standing orientation is 2.35 eV and 3.14 eV, respectively, while an "intermediate" value of the EA for pentacene deposited on a rough ITO surface (thus no clear knowledge of molecular surface orientation) was found to be 2.70 eV.[29,71]

To a first approximation, the energy levels – IE / $E_{ox}$ of the donor and EA / $E_{red}$ of the acceptor – can be used to evaluate if IPA formation is thermodynamically feasible or not. In equilibrium, IPA formation is to occur with high yield when EA > IE or $E_{red} > E_{ox}$, respectively, while it should occur with (very) low yield when EA < IE or $E_{red} < E_{ox}$. In the case of EA ≈ IE or $E_{red} \approx E_{ox}$, IPA formation can proceed with intermediate yield, taking into account thermal energy at room temperature of around 25 meV.

For each set of material combinations, both data-sets predict notably different yields of IPA formation. By comparing the redox-potentials of set I (Figure 1a - left), one would expect that for $D_a$ integer charge transfer is possible with all $F_x$TCNQs, while for $D_b$ IPA formation should occur only with $F_4$TCNQ and $F_2$TCNQ. When comparing IE and EA values (Figure 1a - right), IPA formation of both semiconductors should noticeably occur only with $F_4$TCNQ. For $F_1$TCNQ and $F_2$TCNQ, IPA formation might still be within reach for $D_a$, considering the small IE/EA difference and taking into account the polarization energies of around 100 meV not captured by UPS/IPES (*vide supra*) and by $D^+..A^-$ Coulombic interactions that can stabilize the ion pairs. A comparison of the IE/EA values of set II (Figure 1b - right) shows that, although there is a difference of 500/600 meV between the IE in lying and standing configuration of DH6T/6T, respectively, all IE values are considerably lower than the EA of $Mo(tfd)_3$ and thus IPA formation for DH6T/6T and $Mo(tfd)_3$ should be well possible. However, the reported redox-potentials (Figure 1b - left) suggest IPA formation to be energetically unfavorable. For set III, the reported redox-potentials (Figure 1c - left) suggest integer charge transfer between PFP and $CoCp_2$ to be possible, while the situation of IE/EA values (Figure 1c - right) is more intricate. Here, it is not clear which of the known EA values for standing/lying orientation in films should be given preference when evaluating the possibility of IPA formation, as the relative position of PFP and dopant molecules on the nanoscale is *a priori* unknown or may vary throughout a sample. For PFP in standing configuration the EA is slightly higher than the IE of $CoCp_2$, suggesting that IPA could proceed, but for PFP in lying configuration the EA is significantly lower and IPA formation is expected to be very unlikely. Even when using the intermediate EA for PFP, as approximation for random molecular orientation, it is lower than the reported IE of $CoCp_2$, returning an accordingly low expected IPA yield.

To assess which of these data-sets with opposing predictions on IPA formation yield is more useful, optical absorption spectroscopy measurements were performed, both on solutions and thin films in a molar semiconductor/acceptor ratio of 1:1 (except for set III – see SI). Since neither the semiconductors nor the dopants absorb in the spectral region up to around 1.5 - 2.0 eV, respectively (see Figure 2-4 and Figure S1), features emerging in this spectral region upon mixing can reliably be assigned to ionized semiconductor and/or acceptor molecules by comparison with reference spectra (see SI) and thus give clear evidence for IPA formation.[19] The results of these measurements are summarized in Figures 2-4.

Following the Beer-Lambert law, the fraction of ionized molecules in solution can be obtained from the absorbance of the optical transitions of the respective species, as given in Table 1 for set I and in Table 2 for set II. The optical spectra from solutions of set I (Figure 2a and 2b) show that for nearly half of the material

pairs just a fraction of molecules undergoes ionization, in line with a thermodynamic equilibrium based on the energy difference ΔE of the redox-potentials from CV in Figure 1. By considering the equilibrium relation of single integer charge transfer $\mathrm{D} + \mathrm{A} \rightleftharpoons \mathrm{D}^{+} + \mathrm{A}^{-}$ and following the Nernst equation, the percentage of ionized molecules (P) can be estimated from ΔE taking into account thermal energy at room temperature (for details see SI). As can be seen from Table 1, the theoretically estimated percentages ($P_{theo}$) exhibit reasonable quantitative agreement with the ones estimated from the optical spectra ($P_{exp}$). Differences likely arise from the influences of the electrolyte present during the CV measurements and/or weak ion-pairing effects.

The situation changes when turning towards the solid of set I. While in solution for about half of the semiconductor-dopant combinations only a fraction of the molecules was ionized, the optical spectra of the thin films (Figure 2c and 2d) reveal that in almost every solid system nearly all molecules form IPAs. The clear exception is $D_b$:TCNQ, where only about 1% of the molecules are ionized in the thin film, comparable to the amount found in solution. In the case of $D_b$:$F_1$TCNQ, an estimated 70% of the molecules undergo charge transfer in the solid, which is still much higher than the percentage in solution (about 3%). This transition from partial to (nearly) complete ionization yield was observed to take place during deposition from solution (drop-casting), where the color of the respective samples changed during drying. Consequently, the difference in IPA formation yield for solution versus the solid is to be sought in (small) changes of the effective $E_{ox}$ and $E_{red}$ when changing the state of aggregation. In fact, in solution $E_{ox}$ of $D_b$ is within ca. 100 meV of $E_{red}$ of $F_1$TCNQ and $F_2$TCNQ, so that already small stabilizing effects (e.g., polarization or charge delocalization beyond the initial ion pair) in the solid as compared to solution would suffice to invoke the observed effect; the same applies for the pair $D_a$:TCNQ. Additionally, possible increased planarization of the arylamine groups in the solid might lower $E_{ox}$ of the semiconductor molecules compared to the solution, making IPA with all dopants more probable in thin films. Additional supporting experiments for set I were carried out using the acceptor 11,11,12,12-tetracyano-naphtho-2,6-quinodimethane (TCNNQ) and its fluorinated analog ($F_6$TCNNQ). The results of these measurements are in line with the results presented for the $F_x$TCNQs and are further discussed in the SI.

For set II, the (background corrected) measured spectra summarized in Figure 3 reveal only a tiny fraction of molecules to be ionized. In solution, optical transitions for both ionized DH6T and ionized $Mo(tfd)_3$ can be found (labeled A and B in Figure 3a, respectively), while in the thin film only a transition of ionized 6T is visible (labeled C in Figure 3b) but no clear signature of ionized $Mo(tfd)_3$. The latter is mostly likely due to the weak molar absorptivity of ionized $Mo(tfd)_3$ at around 1.34 eV, being masked by noise and the artefact (marked with X) stemming from the detector change at 1.44 eV of the spectrometer. From these absorption spectra, the fraction of molecules that have undergone electron transfer is estimated to be around 1% for DH6T:$Mo(tfd)_3$ in solution and around 4% for 6T:$Mo(tfd)_3$ in the thin film (for further details see SI). Thus, both in solution and thin film only a small percentage of molecules is ionized. This is in line with the percentage of ionized molecules calculated from the difference in redox-potentials (ca. 20% for DH6T and ca. 3% for 6T), keeping in mind that the reported literature values were measured under slightly different experimental conditions.[51,60]

The experimental conditions used to measure IPA formation yield for set III are different from the other two sets, since in this case it was not possible to achieve a molar 1:1 mixing ratio in solution due to the very low solubility of PFP. Here, we were limited to investigate whether IPA formation is generally possible by exposing PFP to ample amounts of $CoCp_2$, both in solution and thin films (see experimental section and SI for details), the optical spectra of which are summarized in Figure 4. Upon admixture of $CoCp_2$ to a saturated PFP solution, the optical transitions of neutral PFP vanish (labeled C Figure 4a), while a feature at 0.65 eV (labeled A) characteristic of ionized PFP emerges, indicating that nearly all PFP molecules are ionized. In the case of a PFP thin film dipped into a $CoCp_2$ solution (Figure 4b – bottom), the signal of neutral PFP at 1.77 eV vanishes nearly completely, while the feature at 0.73 eV assigned to ionized PFP emerges. The transition appearing at 2.96 eV (labeled E) might be assigned to the $CoCp_2^{+}$ cation by comparison with reference spectra from literature.[63,72]

However, since the absorption of $CoCp_2^+$ is relatively weak[72] and that of $PFP^-$ is expected to be much stronger, the peak at 2.96 eV could also be a higher energy transition of $PFP^-$. In the case of the step-wise sequentially spin-coating of $CoCp_2$ on top of a PFP thin film (Figure 4b – top), the optical transitions of ionized PFP and $CoCp_2$ appear gradually, while at the same time the feature of neutral PFP vanishes, illustrating the possibility of the sequential processing method to control the mixing or doping concentration by choosing appropriate preparation conditions. Both, the spectra of solutions and thin films point towards very efficient IPA formation, although its yield cannot not be quantified based on the present experiments.

The results from set I show that IE and EA values from UPS/IPES do not allow for a reliable estimation of whether IPA is likely to occur for a given material pair (except for the two combinations with the strongest acceptor in this series, $F_4TCNQ$), whereas CV data provide a very reasonable prediction. This can be rationalized when considering that the $F_xTCNQ$s employed here typically form polycrystalline thin films, and substantial effects of molecular arrangement/orientation on IE/EA values are expected due to the numerous highly polar intramolecular bonds; UPS/IPES measurements on uniaxially oriented samples are not available to date. This experimental shortcoming can be seen in comparison with the CV data, where each additional fluorine substitution lowers $E_{red}$ by roughly 100 mV, which is not the case for the solid state EA. For set II, the UPS/IPES data reveal a huge energy offset between the EA of the acceptor and the IE of the donors in favor of charge transfer, while CV data predict the process to be energetically unfavorable, in fact in agreement with experiment. Here, even the knowledge of the difference in IE for different molecular orientations in thin films did not result in improved estimates. For set III, the energy difference in redox-potentials suggests a high IPA formation yield (98%) for PFP with $CoCp_2$, whereas the prediction from UPS/IPES data remains ambiguous. Even when using the intermediate EA of PFP, IPA formation seems energetically unfavorable, in clear contrast to experiment. Thus, the results of set III still support that redox-potentials from CV are more useful for the predicting IPA formation yield. The accuracy of CV-based redox-potentials might be further enhanced by applying ultramicroelectrodes, as this helps reducing effects of electrolytes, and enables measurements with nonpolar solvents and in the solid.[73,74]

**Conclusion**

We explored the practicality of two different material parameters to predict the ion pair formation yield in molecular doping, namely redox-potentials measured by CV in solution versus solid state IE/EA obtained by UPS/IPES on thin films. Three different sets of host-dopant material pairs were investigated, where the redox-potentials and the IE/EA data-sets predict very different yields of ion pair formation. We find that in solution, redox-potentials allow predicting the fraction of neutral and ionized molecules as expected from thermodynamic equilibrium considerations. In thin films, solid state effects apparently change the effective $E_{ox}$ and $E_{red}$ compared to solution, as the IPA formation yield changes compared to solution. However, for the material combinations investigated here, CV data still provide a useful basis to estimate the IPA formation yield in the solid, even though the environment and polarization of ionized molecules in solution and solid is different. In contrast, IE and EA values from UPS/IPES measurements for individual materials in thin films, where the structure is also different from that of the blend, failed to serve as robust parameters to adequately predict IPA formation yield, in many cases even qualitatively. Overall, our results suggest that CV data reveal characteristics on the molecular scale that are relevant for IPA formation in mixed semiconductor-dopant films, whereas IE/EA data include surface and collective electrostatic sample properties, on and above the meso-scale, that do not readily support reliable dopant selection for a given organic semiconductor. This, in fact, is not unexpected for those with extensive experience in the respective methods. However, the use of CV and UPS/IPES as fast "service-type" methods in material science has rapidly increased over the past few years, and the present study is also intended to raise awareness of these pertinent issues. The molar mixing ratio of 1:1 employed in this study is, however, far above dopant concentrations of a few mole-percent as

used in devices (IPA formation yield and thus doping efficiencies are correlated with dopant concentration[19]). Nonetheless, the current findings can be applied for application-relevant material screening as they provide useful trends of the IPA formation yield. A next step to further improve the understanding of molecular doping and its application in organic electronics is to substantiate the relation between ionization yield and doping efficiency, which is yet more challenging.

**Associated Content**

Supporting Information – Further experimental data and thermodynamic considerations.

**Authors Contribution**

BW, AO, SRM, SH, KM, and NK conceived the work, designed the experiments, and supervised the project. BW, LG, and AR performed experiments; YZ, DC, and SB synthesized compounds; BW, AO, and NK prepared the manuscript. All authors commented on the manuscript.

**Author Information**

Corresponding Author:

* norbert.koch@physik.hu-berlin.de

**Acknowledgements**

This work was supported by the Deutsche Forschungsgemeinschaft (DFG) - Projektnummer 182087777 - SFB 951, Projektnummer 286798544 - SA 2916/1-1, and the Helmholtz-Energy-Alliance "Hybrid Photovoltaics". The authors thank Stephan Lüdtke for experimental support. Y.Z., S.B. and S.R.M. thank the U. S. National Science foundation for support of this work, under award No. DMR-1729737. S.R.M. thanks the Alexander von Humboldt Foundation for support of this collaborative work.

**References**

(1) Pfeiffer, M.; Fritz, T.; Blochwitz, J.; Nollau, A.; Plönnigs, B.; Beyer, A.; Leo, K. In *Advances in Solid State Physics 39*; Springer: Berlin, Heidelberg, 1999; Vol. 39.

(2) Gao, W.; Kahn, A. *Appl. Phys. Lett.* **2001**, *79* (24), 4040–4042.

(3) Tanaka, S.; Kanai, K.; Kawabe, E.; Iwahashi, T.; Nishi, T.; Ouchi, Y.; Seki, K. *Jpn. J. Appl. Phys.* **2005**, *44* (6A), 3760–3763.

(4) Zhang, Y.; de Boer, B.; Blom, P. W. M. *Phys. Rev. B* **2010**, *81* (8), 085201.

(5) Olthof, S.; Mehraeen, S.; Mohapatra, S. K.; Barlow, S.; Coropceanu, V.; Brédas, J.-L.; Marder, S. R.; Kahn, A. *Phys. Rev. Lett.* **2012**, *109* (17), 176601.

(6) Leo, K.; Hummert, M. In *Handbook of organic materials for optical and (opto)electronic devices: Properties and applications*; Ostroverkhova, O., Ed.; Woodhead Publishing Limited, 2013.

(7) Di Nuzzo, D.; Fontanesi, C.; Jones, R.; Allard, S.; Dumsch, I.; Scherf, U.; von Hauff, E.; Schumacher, S.; Da Como, E. *Nat. Commun.* **2015**, *6* (1), 6460.

(8) Müller, L.; Nanova, D.; Glaser, T.; Beck, S.; Pucci, A.; Kast, A. K.; Schröder, R. R.; Mankel, E.; Pingel, P.; Neher, D.; Kowalsky, W.; Lovrincic, R. *Chem. Mater.* **2016**, *28* (12), 4432–4439.

(9) Kang, K.; Watanabe, S.; Broch, K.; Sepe, A.; Brown, A.; Nasrallah, I.; Nikolka, M.; Fei, Z.; Heeney, M.; Matsumoto, D.; Marumoto, K.; Tanaka, H.; Kuroda, S.; Sirringhaus, H. *Nat. Mater.* **2016**, *15* (8), 896.

(10) Karpov, Y.; Erdmann, T.; Raguzin, I.; Al-Hussein, M.; Binner, M.; Lappan, U.; Stamm, M.; Gerasimov, K. L.; Beryozkina, T.; Bakulev, V.; Anokhin, D. V.; Ivanov, D. A.; Günther, F.; Gemming, S.; Seifert, G.; Voit, B.; Di Pietro, R.; Kiriy, A. *Adv. Mater.* **2016**, *28* (28), 6003.

(11) D'Andrade, B. W.; Datta, S.; Forrest, S. R.; Djurovich, P.; Polikarpov, E.; Thompson, M. E. *Org. Electron.* **2005**, *6* (1), 11–20.

(12) Djurovich, P. I.; Mayo, E. I.; Forrest, S. R.; Thompson, M. E. *Org. Electron.* **2009**, *10* (3), 515–520.

(13) Arantes, C.; Scholz, M.; Schmidt, R.; Dehm, V.; Rocco, M. L. M.; Schöll, A.; Reinert, F.; Würthner, F. *Appl. Phys. A* **2012**, *108* (3), 629–637.

(14) Savoie, B. M.; Jackson, N. E.; Marks, T. J.; Ratner, M. A. *Phys. Chem. Chem. Phys.* **2013**, *15* (13), 4538.

(15) Sworakowski, J. *Synth. Met.* **2018**, *235*, 125–130.

(16) Li, J.; Duchemin, I.; Roscioni, O. M.; Friederich, P.; Anderson, M.; Da Como, E.; Kociok-Köhn, G.; Wenzel, W.; Zannoni, C.; Beljonne, D.; Blase, X.; D'Avino, G. *Mater. Horizons* **2018**, *6*, 107.

(17) Lüssem, B.; Keum, C.-M.; Kasemann, D.; Naab, B.; Bao, Z.; Leo, K. *Chem. Rev.* **2016**, *116* (22), 13714–13751.

(18) Pingel, P.; Neher, D. *Phys. Rev. B* **2013**, *87* (11), 115209.

(19) Salzmann, I.; Heimel, G.; Oehzelt, M.; Winkler, S.; Koch, N. *Acc. Chem. Res.* **2016**, *49* (3), 370–378.

(20) Cahen, D.; Kahn, A. *Adv. Mater.* **2003**, *15* (4), 271–277.

(21) Woodruff, D. P.; Delchar, T. A. *Modern Techniques of Surface Science*, 2nd ed.; Cambridge University Press: Cambridge, 1994.

(22) Seki, K. *Mol. Cryst. Liq. Cryst. Inc. Nonlinear Opt.* **1989**, *171* (1), 255–270.

(23) Sato, N.; Seki, K.; Inokuchi, H. *J. Chem. Soc. Faraday Trans. 2* **1981**, *77* (9), 1621.

(24) Hwang, J.; Wan, A.; Kahn, A. *Mater. Sci. Eng. R Reports* **2009**, *64* (1–2), 1–31.

(25) Heimel, G.; Salzmann, I.; Duhm, S.; Koch, N. *Chem. Mater.* **2011**, *23* (3), 359–377.

(26) Poelking, C.; Tietze, M.; Elschner, C.; Olthof, S.; Hertel, D.; Baumeier, B.; Würthner, F.; Meerholz, K.; Leo, K.; Andrienko, D. *Nat. Mater.* **2015**, *14* (4), 434–439.

(27) Duhm, S.; Heimel, G.; Salzmann, I.; Glowatzki, H.; Johnson, R. L.; Vollmer, A.; Rabe, J. P.; Koch, N. *Nat. Mater.* **2008**, *7* (4), 326–332.

(28) Salzmann, I.; Duhm, S.; Heimel, G.; Oehzelt, M.; Kniprath, R.; Johnson, R. L.; Rabe, J. P.; Koch, N. *J. Am. Chem. Soc.* **2008**, *130* (39), 12870–12871.

(29) Yoshida, H.; Yamada, K.; Tsutsumi, J.; Sato, N. *Phys. Rev. B* **2015**, *92* (7), 075145.

(30) Bard, A. J.; Faulkner, L. R. *Electrochemical Methods - Fundamentals and Applications*, 2nd ed.; John Wiley & Sons: New York, 2001.

(31) Connelly, N. G.; Geiger, W. E. *Chem. Rev.* **1996**, *96* (2), 877–910.

(32) Pommerehne, J.; Vestweber, H.; Guss, W.; Mahrt, R. F.; Bässler, H.; Porsch, M.; Daub, J. *Adv. Mater.* **1995**, *7* (6), 551–554.

(33) Cardona, C. M.; Li, W.; Kaifer, A. E.; Stockdale, D.; Bazan, G. C. *Adv. Mater.* **2011**, *23* (20), 2367–2371.

(34) Svith, H.; Jensen, H.; Almstedt, J.; Andersson, P.; Lundbäck, T.; Daasbjerg, K.; Jonsson, M. *J. Phys. Chem. A* **2004**, *108* (21), 4805–4811.

(35) Sworakowski, J.; Janus, K. *Org. Electron.* **2017**, *48*, 46–52.

(36) Song, C. K.; Eckstein, B. J.; Tam, T. L. D.; Trahey, L.; Marks, T. J. *ACS Appl. Mater. Interfaces* **2014**, *6* (21), 19347–19354.

(37) Salzmann, I.; Heimel, G. *J. Electron Spectros. Relat. Phenomena* **2015**, *204*, 208–222.

(38) Walzer, K.; Maennig, B.; Pfeiffer, M.; Leo, K. *Chem. Rev.* **2007**, *107* (4), 1233–1271.

(39) Salzmann, I.; Heimel, G.; Duhm, S.; Oehzelt, M.; Pingel, P.; George, B. M.; Schnegg, A.; Lips, K.; Blum, R.-P.; Vollmer, A.; Koch, N. *Phys. Rev. Lett.* **2012**, *108* (3), 035502.

(40) Torrance, J. B. *Acc. Chem. Res.* **1979**, *12* (3), 79–86.

(41) Jacobs, I. E.; Cendra, C.; Harrelson, T. F.; Bedolla Valdez, Z. I.; Faller, R.; Salleo, A.; Moulé, A. J. *Mater. Horizons* **2018**, *5* (4), 655–660.

(42) Neelamraju, B.; Watts, K. E.; Pemberton, J. E.; Ratcliff, E. L. *J. Phys. Chem. Lett.* **2018**, *9* (23), 6871–6877.

(43) Thomas, E. M.; Davidson, E. C.; Katsumata, R.; Segalman, R. A.; Chabinyc, M. L. *ACS Macro Lett.* **2018**, *7* (12), 1492–1497.

(44) Jeon, N. J.; Lee, J.; Noh, J. H.; Nazeeruddin, M. K.; Grätzel, M.; Seok, S. Il. *J. Am. Chem. Soc.* **2013**, *135* (51), 19087–19090.

(45) Nie, H.-J.; Yao, C.-J.; Shao, J.-Y.; Yao, J.; Zhong, Y.-W. *Chem. - A Eur. J.* **2014**, *20* (52), 17454–17465.

(46) Garnier, F.; Yassar, A.; Hajlaoui, R.; Horowitz, G.; Deloffre, F.; Servet, B.; Ries, S.; Alnot, P. *J. Am. Chem. Soc.* **1993**, *115* (19), 8716–8721.

(47) Dodabalapur, A.; Torsi, L.; Katz, H. E. *Science.* **1995**, *268* (5208), 270–271.

(48) Halik, M.; Klauk, H.; Zschieschang, U.; Schmid, G.; Ponomarenko, S.; Kirchmeyer, S.; Weber, W. *Adv. Mater.* **2003**, *15* (11), 917–922.

(49) Loi, M. A.; da Como, E.; Dinelli, F.; Murgia, M.; Zamboni, R.; Biscarini, F.; Muccini, M. *Nat. Mater.* **2004**, *4* (1), 81–85.

(50) Duhm, S.; Xin, Q.; Koch, N.; Ueno, N.; Kera, S. *Org. Electron.* **2011**, *12* (6), 903–910.

(51) Qi, Y.; Sajoto, T.; Barlow, S.; Kim, E.-G.; Brédas, J.-L.; Marder, S. R.; Kahn, A. *J. Am. Chem. Soc.* **2009**, *131* (35), 12530–12531.

(52) Tiwari, S. P.; Potscavage, W. J.; Sajoto, T.; Barlow, S.; Marder, S. R.; Kippelen, B. *Org. Electron.* **2010**, *11* (5), 860–863.

(53) Sakamoto, Y.; Suzuki, T.; Kobayashi, M.; Gao, Y.; Fukai, Y.; Inoue, Y.; Sato, F.; Tokito, S. *J. Am. Chem. Soc.* **2004**, *126* (26), 8138–8140.

(54) Inoue, Y.; Sakamoto, Y.; Suzuki, T.; Kobayashi, M.; Gao, Y.; Tokito, S. *Jpn. J. Appl. Phys.* **2005**, *44* (6A), 3663–3668.

(55) Chan, C. K.; Amy, F.; Zhang, Q.; Barlow, S.; Marder, S.; Kahn, A. *Chem. Phys. Lett.* **2006**, *431* (1–3), 67–71.

(56) Davison, A.; Holm, R. H.; Benson, R. E.; Mahler, W. In *Inorganic Syntheses*; 2007; Vol. 10, pp 8–26.

(57) Chercka, D. Dissertation - Pyrene Derivatives as Donors and Acceptors, Johannes Gutenberg-Universität Mainz, 2014.

(58) Scholes, D. T.; Hawks, S. A.; Yee, P. Y.; Wu, H.; Lindemuth, J. R.; Tolbert, S. H.; Schwartz, B. J. *J. Phys. Chem. Lett.* **2015**, *6* (23), 4786–4793.

(59) Kanai, K.; Akaike, K.; Koyasu, K.; Sakai, K.; Nishi, T.; Kamizuru, Y.; Nishi, T.; Ouchi, Y.; Seki, K. *Appl. Phys. A* **2009**, *95* (1), 309–313.

(60) Facchetti, A.; Yoon, M.-H.; Stern, C. L.; Hutchison, G. R.; Ratner, M. A.; Marks, T. J. *J. Am. Chem. Soc.* **2004**, *126* (41), 13480–13501.

(61) Ivanco, J.; Haber, T.; Krenn, J. R.; Netzer, F. P.; Resel, R.; Ramsey, M. G. *Surf. Sci.* **2007**, *601* (1), 178–187.

(62) Duhm, S.; Salzmann, I.; Koch, N.; Fukagawa, H.; Kataoka, T.; Hosoumi, S.; Nebashi, K.; Kera, S.; Ueno, N. *J. Appl. Phys.* **2008**, *104* (3), 033717.

(63) Bockman, T. M.; Chang, H. R.; Drickamer, H. G.; Kochi, J. K. *J. Phys. Chem.* **1990**, *94* (22), 8483–8493.

(64) Wang, K.; McConnachie, J. M.; Stiefel, E. I. *Inorg. Chem.* **1999**, *38* (19), 4334–4341.

(65) Sakamoto, Y.; Komatsu, S.; Suzuki, T. *J. Am. Chem. Soc.* **2001**, *123* (19), 4643–4644.

(66) Tian, H.; Wang, J.; Shi, J.; Yan, D.; Wang, L.; Geng, Y.; Wang, F. *J. Mater. Chem.* **2005**, *15* (29), 3026.

(67) Ge, Y.; Whitten, J. E. *Chem. Phys. Lett.* **2007**, *448* (1–3), 65–69.

(68) Opitz, A.; Frisch, J.; Schlesinger, R.; Wilke, A.; Koch, N. *J. Electron Spectros. Relat. Phenomena* **2013**, *190*, 12–24.

(69) Kahn, A.; Koch, N.; Gao, W. *J. Polym. Sci. B* **2003**, *41*, 2529–2548.

(70) Ivanco, J.; Netzer, F. P.; Ramsey, M. G. *J. Appl. Phys.* **2007**, *101* (10), 103712.

(71) Han, W.; Yoshida, H.; Ueno, N.; Kera, S. *Appl. Phys. Lett.* **2013**, *103* (12), 123303.

(72) Barlow, S. *Inorg. Chem.* **2001**, *40* (27), 7047–7053.

(73) Wightman, R. M. *Anal. Chem.* **1981**, *53* (9), 1125A-1134A.

(74) Heinze, J. *Angew. Chemie Int. Ed. English* **1993**, *32* (9), 1268–1288.

## Figures and Tables

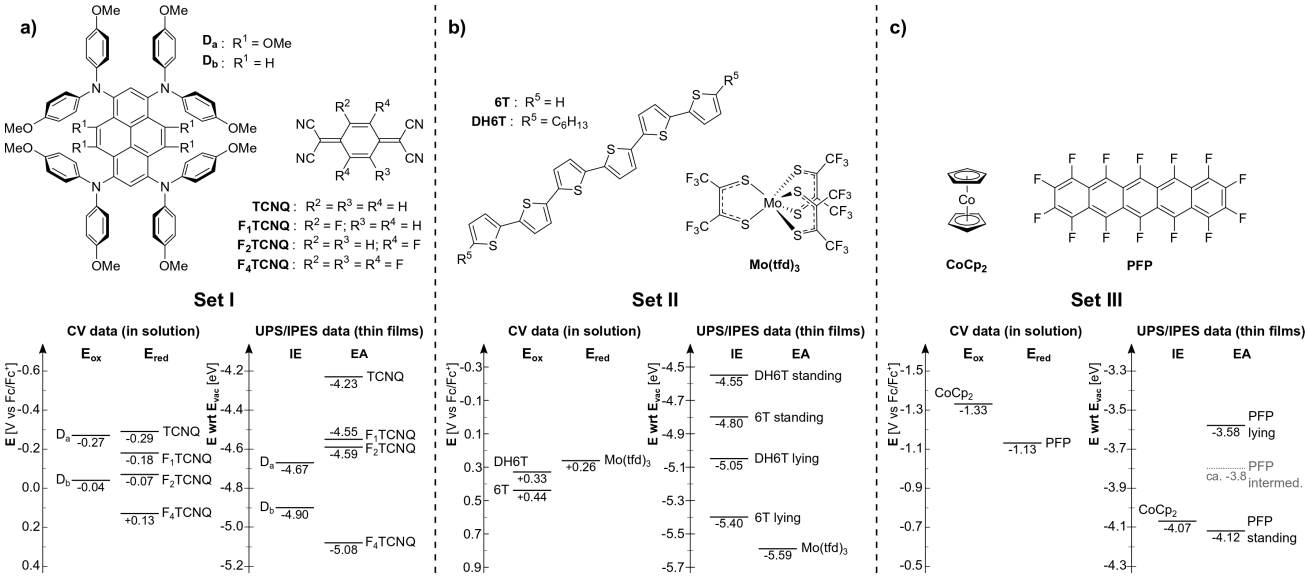


**Figure 1.** Chemical structures (top) and energy level diagrams deduced from CV and UPS/IPES data (bottom) of the used materials. **a)** Set I: Donor hosts 1,3,6,8-tetra[bis(*p*-anisyl)amino]-4,5,9,10-tetramethoxypyrene ($D_a$) / 1,3,6,8-tetra[bis(*p*-anisyl)amino]pyrene ($D_b$) and acceptor dopants, tetracyanoquinodimethane and fluorinated derivatives ($F_x$TCNQ). Redox-potentials and IE were measured in this work, EA of $F_x$TCNQs taken from literature.[59] **b)** Set II: Donor hosts α-sexithiophene (6T) / α,ω-dihexylsexithiophene (DH6T) and acceptor dopant molybdenum tris[1,2-bis(trifluoromethyl)ethane-1,2-dithiolene] ($Mo(tfd)_3$). Energy levels were taken from literature.[51,60–62] **c)** Set III: Acceptor host perfluoropentacene (PFP) and donor dopant cobaltocene ($CoCp_2$). Energy levels were taken from literature[29,31,53,55] and the intermediate EA for PFP (grey) was estimated by comparison of the EA of pentacene in different orientations.[29,71]

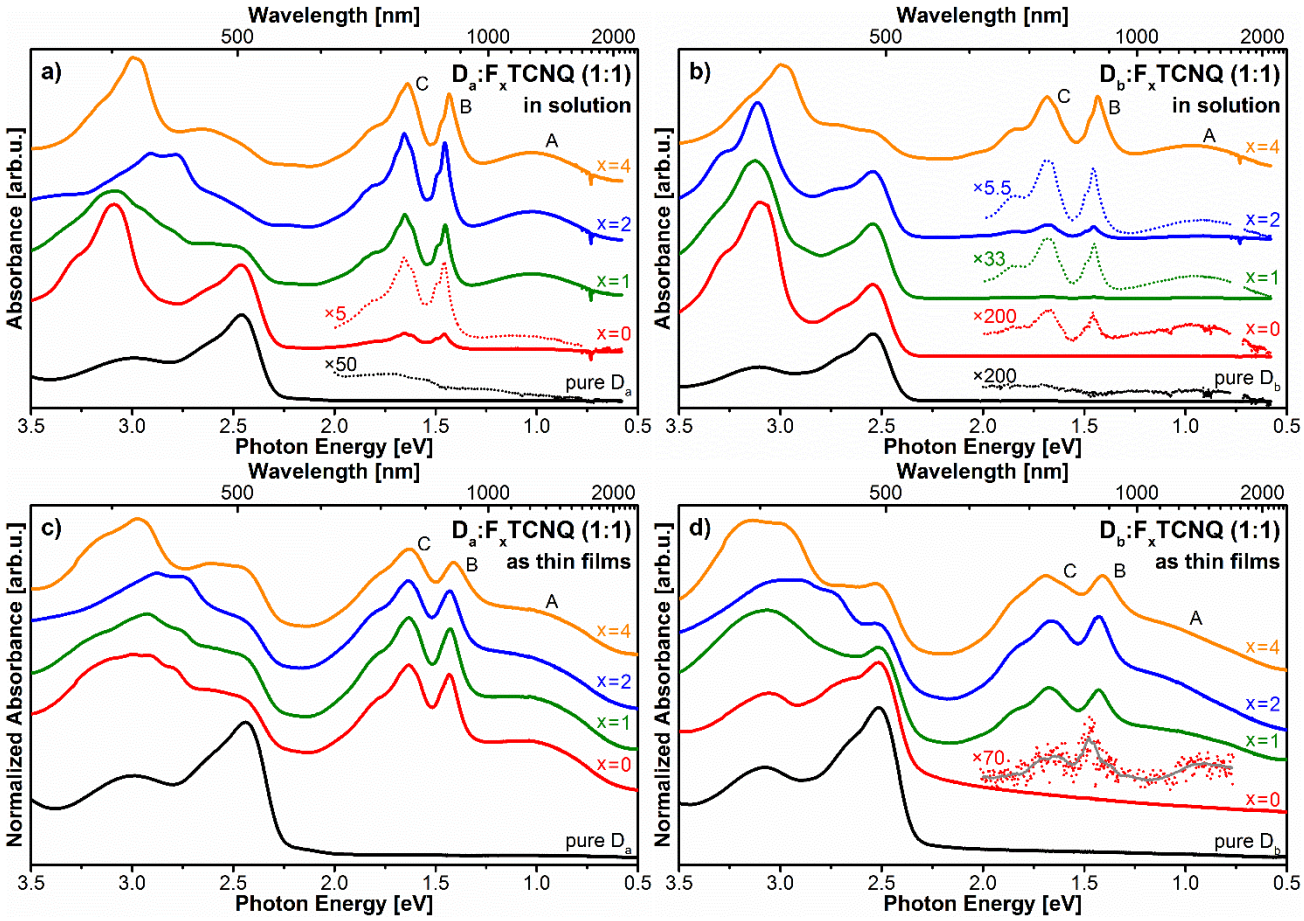


**Figure 2.** Optical absorption spectra of **a)** $D_a$:$F_x$TCNQ in solution, **b)** $D_b$:$F_x$TCNQ in solution, **c)** $D_a$:$F_x$TCNQ in thin films, and **d)** $D_b$:$F_x$TCNQ in thin films. For clarity, reference spectra of the pure $F_x$TCNQ are not depicted (they can be found in the SI). By comparison with reference spectra (see SI), the new emerging peaks in the range of 0.5 to 2.0 eV can be attributed to the cation features of $D_x$ (A), the anion features of $F_x$TCNQ (B), and a superposition of both (C). The solution spectra show that only for $D_a$:$F_2$TCNQ, $D_a$:$F_4$TCNQ and $D_b$:$F_4$TCNQ nearly all molecules are ionized, while in the other combinations only a fraction does. In thin films for all combinations (except for $D_b$:TCNQ) nearly all dopant molecules are ionized. For combinations with low ionization yield, the spectral region ca. 0.5 - 2.0 eV is magnified for better visibility (dashed lines). For thin film $D_b$:TCNQ, a background was subtracted in this spectral region and the data was smoothened because of the small signal-to-noise ratio (grey line).

**Table 1.** Theoretical IPA formation percentage ($P_{theo}$) as function of the difference in electrochemical potential (ΔE) in comparison with measured yield of ionized molecules in solution ($P_{exp}$). Both show the same trend and are in reasonable quantitative agreement.

| | **ΔE [mV]** | | **$P_{theo}$ [%]** | | **$P_{exp}$ [%]** | |
|---|---|---|---|---|---|---|
| | **$D_a$** | **$D_b$** | **$D_a$** | **$D_b$** | **$D_a$** | **$D_b$** |
| **TCNQ** | -22 | -246 | 39 | 0.8 | 20 | 0.5 |
| **$F_1$TCNQ** | 89 | -135 | 85 | 7 | 75 | 3 |
| **$F_2$TCNQ** | 197 | -27 | 98 | 37 | 100 | 18 |
| **$F_4$TCNQ** | 398 | 174 | 100 | 97 | 100 | 100 |

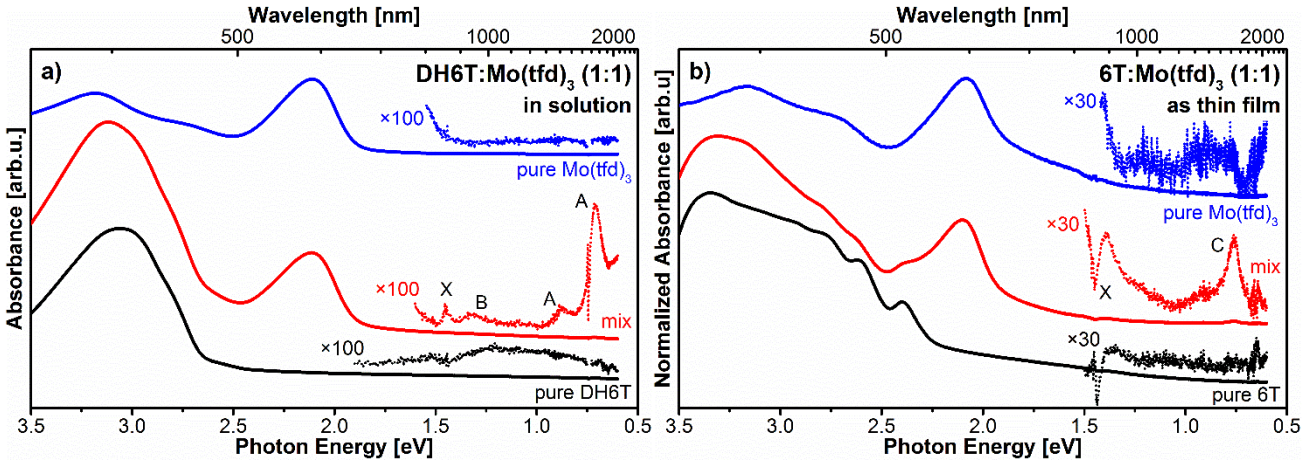


**Figure 3.** Optical absorption spectra of **a)** DH6T:$Mo(tfd)_3$ in solution, and **b)** a 6T:$Mo(tfd)_3$ thin film. A background was subtracted in the spectral region of ca. 0.5 to 1.5 eV (see experimental section for details) and magnified for better visibility (dashed lines). The features appearing in mixtures are assigned to ionized DH6T (A), ionized $Mo(tfd)_3$ (B), and ionized 6T (C) by comparison with reference spectra (see SI). The signal at 1.44 eV (X) is an artefact from detector-change during measurement. The spectra of the mixed material samples reveal only a minute fraction of molecules being ionized.

**Table 2.** Theoretical IPA formation percentage ($P_{theo}$) as function of the difference in electrochemical potential (ΔE) in comparison with measured yield of ionized molecules ($P_{exp}$), for DH6T in solution ($DH6T^{sol}$) and 6T in thin films ($6T^{TF}$).

| | ΔE [mV] | | $P_{theo}$ [%] | | $P_{exp}$ [%] | |
|---|---|---|---|---|---|---|
| | DH6T | 6T | DH6T | 6T | $DH6T^{sol}$ | $6T^{TF}$ |
| $Mo(tfd)_3$ | -70 | -180 | 20 | 3 | 1 | 4 |

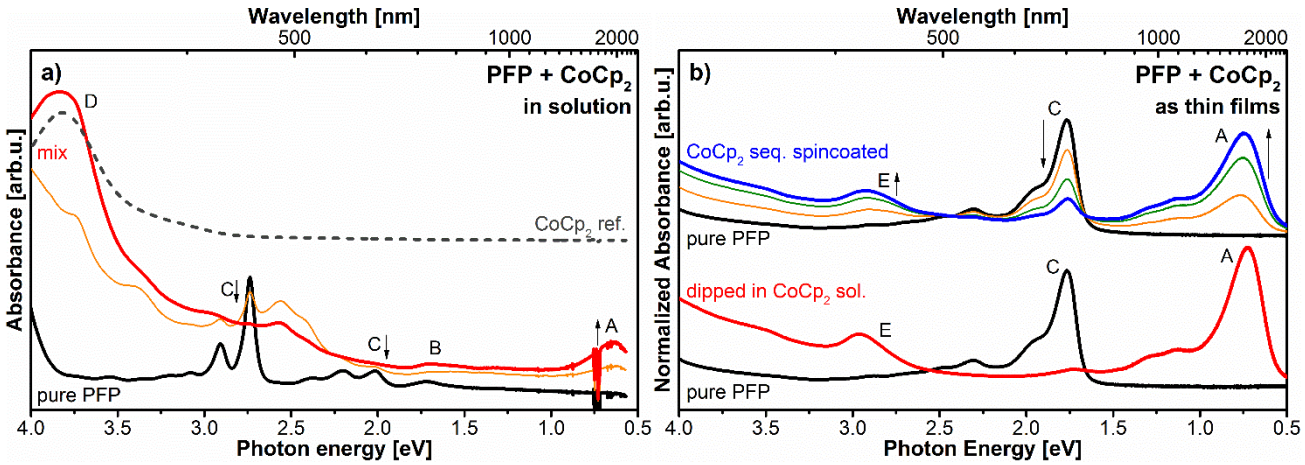


**Figure 4.** Optical absorption spectra of **a)** PFP mixed with (excess) $CoCp_2$, and **b)** PFP thin films, dipped in a $CoCp_2$ solution (bottom) and prepared *via* sequential spin-coating (top). In a) the mixed solution of the red curve contains double the amount of $CoCp_2$ than the one of the orange curve; this was done in order to achieve and visualize higher ionization of the PFP molecules. The optical transitions appearing upon mixing in solution are assigned to ionized PFP (A – see SI) and neutral $CoCp_2$ (D), while the features of neutral PFP (C) are

vanishing. The transitions at around 1.7 eV (B) belong to non-dissolved PFP in the saturated PFP solutions and are not changing significantly upon mixing. In thin films, the newly appearing feature at around 2.96 eV (E) might be assigned to ionized $CoCp_2$ by comparison with literature spectra.[63,72] (However, the peak at 2.96 eV could also be a higher energy transition of $PFP^-$ coincidently at the same position as $CoCp_2^+$ – see text). Although the IPA formation yield cannot be quantified here, the spectra suggest IPA formation of $PFP^-$:$CoCp_2^+$ to be efficient.

**TOC – Figure**

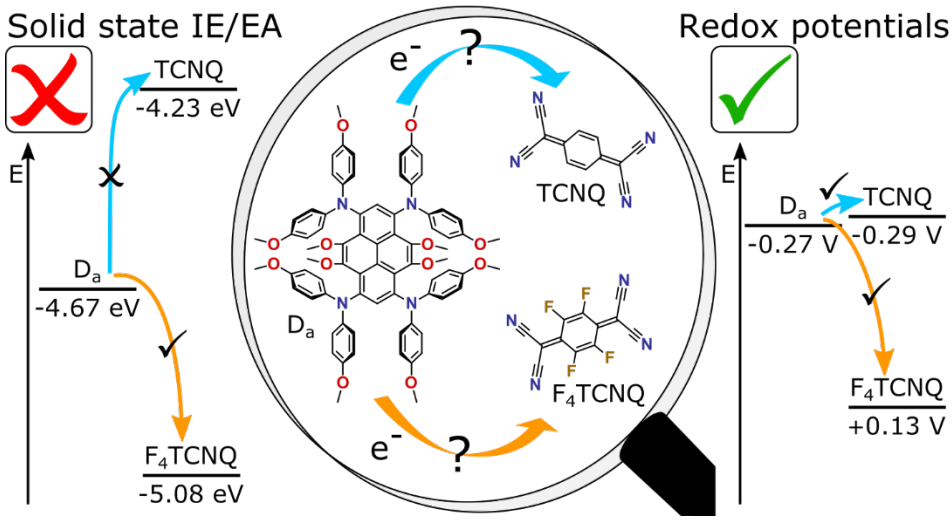
Solid state IE/EA
TCNQ
-4.23 eV
E
D$_a$
-4.67 eV
F$_4$TCNQ
-5.08 eV
e$^-$
?
TCNQ
D$_a$
F$_4$TCNQ
e$^-$
?
Redox potentials
E
D$_a$
-0.27 V
TCNQ
-0.29 V
F$_4$TCNQ
+0.13 V